Available Online at http://www.journalajst.com

ASIAN JOURNAL OF SCIENCE AND TECHNOLOGY

ISSN: 0976-3376

Asian Journal of Science and Technology
Vol. 15, Issue, 11, pp. 13183-13188, November, 2024

RESEARCH ARTICLE

A STUDY OF THE EFFECTS OF SiN TREATMENT ON THE GaN REFRACTIVE INDEX

[*1]Waten Chalabi, [2]Laifi, J., [1]Bchetnia, A. and [3]Lafford, T.A.

[1]Department of Physics, College of Science, Qassim University, Saudi Arabia
[2]Physics Department, College of Science, Jouf University, P.O. Box 2014, Sakaka, Saudi Arabia
[3]Bruker Corporation, Billerica, United States

ARTICLE INFO

Article History:
Received 14th August, 2024
Received in revised form
28th September, 2024
Accepted 16th October, 2024
Published online 23rd November, 2024

Keywords:
GaN, SiN treatment, Ellipsometry, Optical properties.

ABSTRACT

In the present study, both the GaN buffer layer approach and the sapphire SiN treatment method were used to develop GaN films by metalorganic chemical vapor deposition (MOCVD) on a c-plane (0001) sapphire substrate. The growth was controlled in situ by 632.8 nm laser reflectometry. The GaN-grown layer structure wasinvestigated via high-resolution X-ray diffraction (HRXRD). TheGaN structural properties improved upon SiN treatment. In addition, spectroscopic transmittance was used to determine the change in the bandgap energy of GaN upon SiN treatment.Spectroscopic ellipsometric (SE) data (ψ and Δ) acquired in the wavelength range 400-1700 nm, were analyzed using a multilayer approach. The extracted refractive indices were found to follow a Cauchy-type dispersion. Upon SiN treatment, there is a blueshift and a decrease in the refractive index. At 600 nm, the GaN refractive index decreases from 2.395 to 2.374. The SE refractive indices measurements agree with the spectroscopic reflectometry (SR) results.

Citation: ***Waten Chalabi, Laifi, J., Bchetnia, A. and Lafford, T.A.*** **2024.** "A study of the effects of SiN treatment on the GaN refractive index", *Asian Journal of Science and Technology*, 15, (11), 13183-13188.

INTRODUCTION

GaN and related compounds have recently made strides in both epitaxial and bulk growth, making them competitive candidates for a wide range of applications, including visible light emitters (for which III-nitride-based technology has already been commercialized) and high-frequency and high-power devices.It is common knowledge that group III nitrides have the following properties: They span a broad bandgap from 6.2 eV (AlN) to 0.7 eV (InN) (Miyoshi *et al*., 2009). The mechanical stability of these materials is attributed to their higher binding energies than those of other materials. GaN exhibits favorable electron transport characteristics, making it a desirable material for high-frequency applications. Its electron mobility may exceed 2000 cm^2/V s, and its average electron saturation velocity is more than 2×10^7 cm/s (Kyle, 2014). Nitrides are generally advantageous for use in high-temperature, high-frequency, and high-power applications in hazardous situations. However, since there is currently no commercially available substrate for homoepitaxy, single-crystalline GaN films still need to be grown heteroepitaxially on substrates such as sapphire or SiC, which more or less closely match the lattice constants and thermal expansion coefficients of these materials. Numerous investigations have demonstrated that direct GaN growth on a sapphire substrate leads to a poorly crystalline structure due to incomplete substrate wetting. High-quality epilayers of III-nitrides on sapphire substrates can be grown by MOCVD in two steps (Amano, 1986). Nitrides were grown using a two-step procedure by Amano et al. (Amano, 1988), which involved first growing an AlN buffer layer at 800°C and then a GaN layer at a high temperature. As a result, the surface morphology was enhanced, and the defect density was significantly decreased.

The buffer layer provides a high density of nucleation centers and promotes the lateral growth of the main epilayer. A GaN nucleation layer was employed at 600 C by Nakamura, 1991. As a result, there is less stress and lower fault density. However, in the elaborated layers, a high dislocation density (10^{10}–11^{11}/cm2) remained. We previously observed that the quality of GaN is greatly improved when SiN treatment is applied to a sapphire substrate (Bchetnia, 2007). Indeed, through this process, the first stages of growth begin with a three-dimensional (3D) nucleation mode, subsequently favoring the lateral growth rate of GaN, transitioning to a two-dimensional (2D) mode (Benzarti, 2004). This simple and inexpensive process makes it possible to effectively reduce the density of emerging dislocations, thus significantly improving the efficiency of optoelectronic devices (Edwards, 2005). Haffouz et al. (Haffouz, 2001), reported that in situ SiN treatment of sapphire substrates improved the optical properties of GaN grown by MOCVD. Recently, Benzarti et al. (2017), reported an increase in the blue emission of MQW LEDs using SiN treatment compared to that of the same MQW device grown on a conventional GaN buffer layer.

To further improve GaN-based optoelectronic device performance, good knowledge of refractive indices is needed. Spectroscopy ellipsometry (SE) is a great technique for characterizing multilayered structures, providing the thickness, composition, and optical properties of each layer (Sullivan, 1988). Until now, a few investigations on SE studies of GaN have been performed (Yu, 1997; Yang, 1998; Yu, 1997; Kawashima, 1997 and Siozade, 2000). Panda et al. (Panda, 2021), reported a significant change in the complex refractive index of AlN by doping with Ti and Cr. Furthermore, Zauner et al. (1998) reported a difference between the refractive indices of bulk and heteroepitaxial GaN. The SiN treatment seems to have a considerable effect on the GaN structural, electrical, and

optical properties. However, little attention has been devoted to this topic. In this study, two GaN samples elaborated with and without SiN treatment were grown on (00.1) sapphire substrates by metalorganic chemical vapor deposition (MOCVD). The effects of SiN treatment on GaN properties were investigated by in situ laser reflectometry, spectroscopy ellipsometry (SE), HRXRD, and spectroscopy reflectivity (SR). These results will aid in the design and simulation of GaN-based optoelectronics, such as blue light-emitting diodes and Bragg mirrors.

Experiments: Using a vertical atmospheric pressure MOCVD reactor, GaN layers were grown on a one-sided polished (0001) sapphire substrate at 1120°C with and without SiN treatment. The growth layers were approximately 1.6 µm thick. The growth was controlled in situ with He-Ne laser reflectometry (λ= 632.8 nm). More information about the growth process was published elsewhere (Bchetnia, 2007 and Benzarti, 2004). X-ray measurements were performed with a high-resolution diffractometer equipped with a fourfold Ge (220) monochromator, delivering a pure CuKα_1 line of wavelength (λ= 0.154 nm).Variable-angle spectral ellipsometry (SE) was carried out using Glan Taylor polarizers (J. A. Woollam Co.) and an electronically controlled rotating compensator at room temperature in the ambient atmosphere.The GaN crystals were subsequently characterized by UV-vis spectroscopy (PerkinElmer Lambda 950), and spectroscopy reflectometry (Thinfilmetric F20). All the measurements were performed at room temperature.

RESULTS AND DISCUSSION

The laser reflectivity insitu monitoring signals during the growth of the two studied samples with (sample S1) and without SiN treatment (sample S2) are shown in Figure 1.

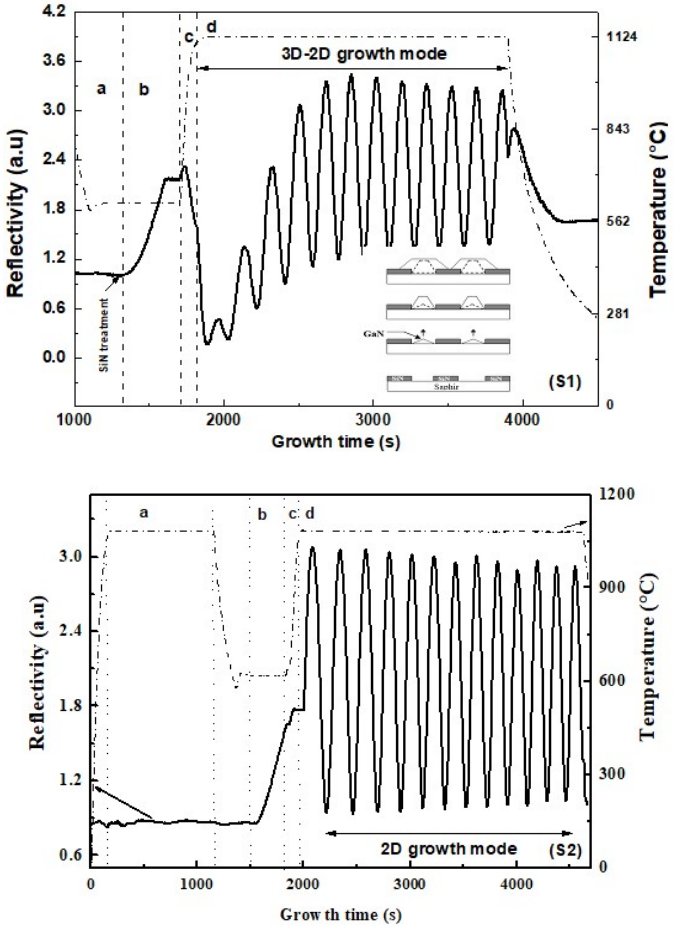

Figure 1. In-situ real-time laser reflectometry recorded during the growth of the two studied GaNsamples with (S1) and without (S2) SiN treatment. The insert in the S1 reflectometry image shows a schematic diagram of the SiN treatment

The different growth stages labeled (a, b, c, and d) in Figure 1 represent nitridation, buffer layer growth, a temperature increase from 600 to 1120 C, and GaN epilayer growth, respectively. Before starting the GaN growth process (stage a), the sapphire substrate was nitridated for 10 min under an NH_3+H_2+N_2 atmosphere at 1120°C for the two samples. In the case of SiN-treated sample S1, at 1120 °C, a random SiNnanomask was applied by exposing the nitridated sapphire to a mixture of NH_3 and SiH_4 for 75 seconds. Next, a 30 nm GaN buffer layer was deposited at 600 °C for the two samples (stage b). The subsequent Ga precursor (trimethyl-gallium: TMG) is turned OFF, and the temperature is ramped up to 1120 °C (stage c). When the growth temperature is reached, the start of GaN epilayer growth is marked by the turning ON of TMG flow. N2 is turned off for sample S1, the NH3 flow rate is maintained at 2 slm, and the H2 flow rate is increased to 4 slm. The effect of SiNnanomask deposition was observed during growth, as shown in Figure 1. In fact, in the case of the sapphire SiN treatment, the reflectivity signals significantly drop and start to oscillate (stage 3D), a synonym of the 3D growth mode. Afterward, the coalescence of the 3D islands progresses, and the amplitude of oscillations increases, a synonym of the 3D-2D transition mode. The inset schematic diagram in Figure 1 illustrates the effect of SiN treatment on the GaN epilayer growth mode (Fitouri, 2005). For sample S2 grown without SiN treatment, during GaN epilayer growth, the NH_3 flow rate remained at 2 slm, and the N_2 flow rate was increased to 4 slm while the H_2 flow was switched off. The growth is governed by the 2D deposition mode from the beginning, as shown by the constant oscillation amplitude of the in situ reflectivity. From the in-situ reflectometry average period oscillations (Fitouri, 2005), the growth rates of samples S1 and S2 were found to be approximately 2.77 µm/h and 2.25 µm/h, respectively. Differences in growth rates, coalescence processes, and gas mixtures could affect the physical properties of epitaxial layers S1 and S2. Ex-situ characterizations were performed to study the effect of SiN treatment on the optical and structural qualities of S1 and S2. A GaN HRXRD symmetric 2θ-w scan is shown in Figure 2.

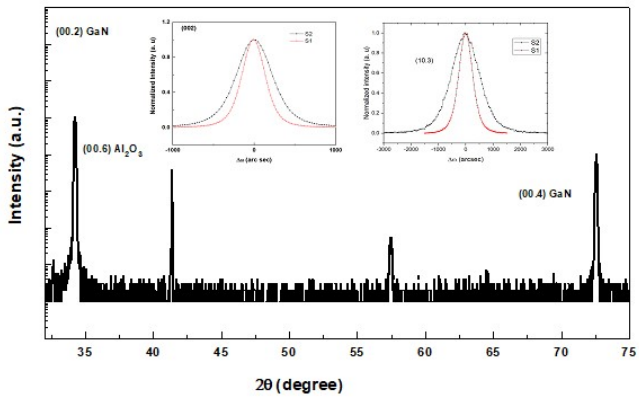

Figure 2. HRXRD symmetric 2θ-w scans of samples with (S1) and without (S2) SiN treatment. The inserts show the rocking curve scan modes from the symmetric (00.2) and asymmetric (10.3) planes for the two prepared samples

Samples S1 and S2 exhibited the same diffraction patterns. Three main diffraction peaks are recorded and labeled. The peaks located at 34.473°, 41.4°, and 72.809° are attributed to the diffraction of GaN (00.2), sapphire (00.6), and GaN (00.4), respectively. The extremely crystalline GaN film formed epitaxially along the c-direction on the c-plane sapphire substrate was demonstrated by the apparent existence of first and second-order X-ray diffractions of GaN in the 2θ-w scan. Additionally, the dislocation density and crystalline quality of the GaN epitaxial layer were obtained via HRXRD. The rocking curve scans from the symmetric (00.2) planes of samples S1 and S2, with FWHMs of 290 and 440 arcsec, respectively, are displayed in the inset of Figure 2. The rocking curve broadening was used to estimate the screw dislocation density (D_{screw}) by using the following relation:

$$D_{screw} = \frac{FWHM^2_{(00.2)}}{9\,b^2_{screw}}\ [6] \qquad \text{.....(1)}$$

where b is the burger vector length (b_{screw}=0.3189 nm).

The calculated screw dislocation densities are 5 10^8 cm^{-2} for S2 and2.4 10^8 cm^{-2} for S1, which are the same magnitude as those previously reported (Li, 2022). Zhu et al. (1996) reported that the spectra of symmetric reflections (00.l) are broadened only by screw dislocations and the screw component of mixed dislocations, while those of asymmetric reflections are broadened by edge dislocations and the edge component of mixed dislocations. Thus, for samples S1 and S2, asymmetric (h0.l) w-scans were performed. An example of the 10.3 rocking curve scan mode was inserted in the figure. The broadening reduction upon SiN treatment was enhanced. (10.3) The FWHM was reduced from 1057 to 629 arcsec. This reduction is approximately three times greater than that observed for the symmetric (00.2) reflection. SiN treatment affects different edge and screw dislocations. Indeed, the GaN lateral coalescence process favored by SiN treatment causes horizontal propagation of emerging dislocations (Böttcher, 1976). This curvature of the dislocation lines is probably more pronounced for edge dislocations.On the other hand, it was reported that the use of a thin initial SiN layer makes it possible to form GaN islands. Although these islands are statistically more disoriented than are two-dimensional layers deposited on sapphire, the distance between them is much greater than that in the case of 2D growth. The islands therefore form wide columns, thus reducing the density of defects created at grain subboundaries (Vickers, 2005). The optical transmission spectra of S1 and S2 are displayed in Figure 3.

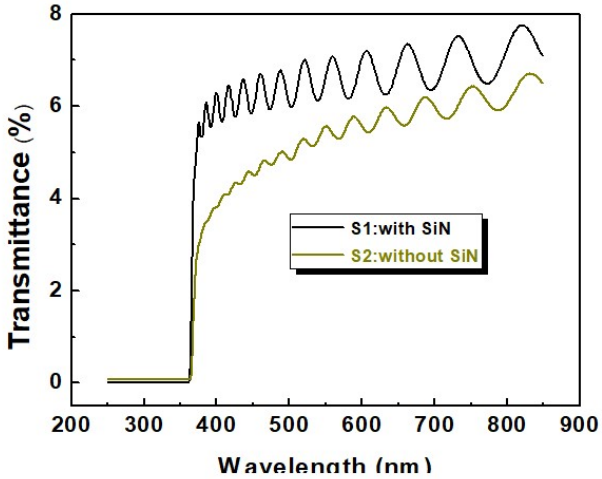

Figure 3. Optical transmission spectra of the samples with (S1) and without (S2) SiN treatment

This figure shows that sample S2 slowly increased, whereas sample S1 exhibited highly crisp wavelength cutoff curves, suggesting that the crystal quality of sample S1 is superior to that of sample S2 in good agreement with the HRXRD results. Oscillations are frequently apparent in the transmittance of samples in the visible region due to the interference effect between the sapphire substrate and GaN. These oscillations may be exploited for the extraction of film thickness. The wavelengths λ1 and λ2, which are given by the following equation, correspond to the neighboring minimum or maximum of the interference component in the reflection spectrum in the case of normal incidence of light:

$$2n_1 d = m\lambda_1 \qquad \text{.....(2)}$$

$$2n_2 d = (m+1)\lambda_2 \qquad \text{.....(3)}$$

where d is the thickness of the GaN layer, m is the oscillation peak order, and n1 and n2 are the refractive indices of GaN for the wavelengths λ1 and λ2, respectively.

From the above equations, the film thickness could be calculated for each period by the following equation (Vidal, 1996):

$$d = \frac{\lambda_1\,\lambda_2}{[2(n_1\lambda_2 - n_2\lambda_1)]} \qquad \text{.....(4)}$$

The refractive index for each wavelength is taken from reference (Zauner, 1998). The average S1 and S2 film thicknesses obtained from interference oscillations in the transparent region near 600 nm are approximately 1.448 and 1.624 µm, respectively, which are near those obtained from in-situ reflectometry measurements.

The absorption coefficient could be deduced from the transmittance measurements as follows:

$$\alpha(\hbar\nu) = -\frac{1}{d}\ln T(\hbar\nu) \qquad \text{.....(5)}$$

The values of the energy gap for S1 and S2 were calculated using the Tauc plot for direct bandgap semiconductors (Jubu, 2020):

$$\alpha^2 = A(\hbar\nu - E_g) \qquad \text{.....(6)}$$

where A is a constant and E_g is the energy gap.

The bandgap energy is determined using eq. (6) via linear regression analysis close to the absorption edge. The calculated values of the absorption coefficient are shown in Figure 4.

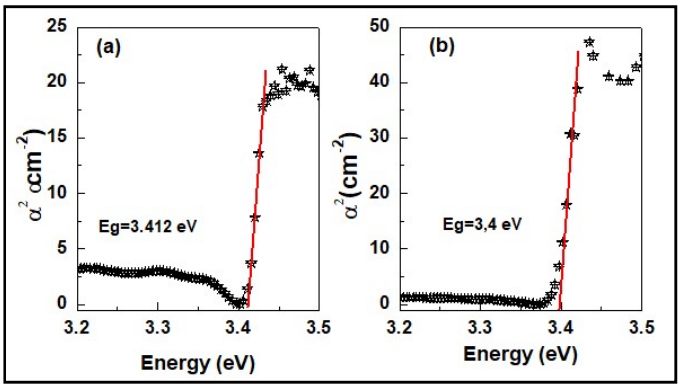

Figure 4. Absorption coefficient deduced from the transmittance measurements of the samples with (a) and without (b) SiN treatment

The obtained values are 3.4 and 3.41 eV for samples S2 and S1, respectively. The blueshift observed upon SiN treatment is associated with an increase in residual stress, as was reported in reference (Haffouz, 2001). SE was performed on the GaN layers to investigate the effect of SiN treatment on the refractive index. The ellipsometry measurements were carried out in the spectral range of 400-1700 nm at room temperature. We performed SE at three incident angles of 55°, 60° and 65°. Figures 5 (a) and (b) show the obtained experimental (scatter) ψ (λ) and Δ(λ) for the two samples S1 and S2, respectively. The obtained ellipsometric data were analyzed with the help of the fitting software Complete Ease (A J. A Woollam Co.). The mean square error (MSE) determines the fit quality. To achieve the best fit result, a four-phase model (ambient/roughened GaN/GaN/Al2O3) was employed. The substrate backside was unpolished, thus, the light backside reflection contribution to the ψ and Δ values was neglected.In the transparent region above the GaN bandgap, interference oscillations appeared. The film thickness, d, obtained by fitting to the UV-Vis data, was subsequently used to obtain refined values of the refractive indices from the SE data. The real part of the GaN refractive indices was analyzed using a Cauchy-type model of dispersion given by:

$$n(\lambda) = A + \frac{}{\lambda^2} + \frac{}{\lambda^4} \qquad \text{.....(7)}$$

where A, B, and C are fitting parameters and λ is the wavelength in nanometers.

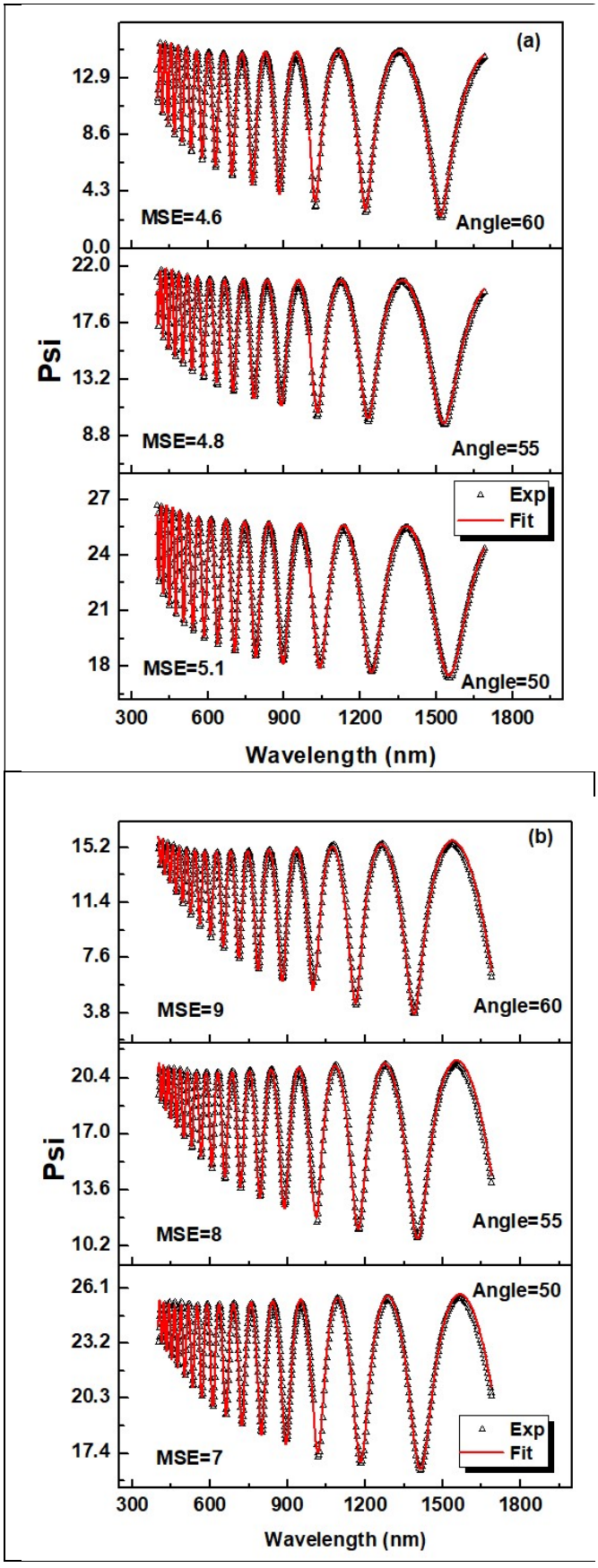

Figure 5. Experimental data of ψ (λ) and Δ (λ) of the two samples with (a) and without (b) SiN treatment. The red solid lines present the fit of the experimental data

The fitting results are shown as solid lines in Figures 5 (a) and (b). A good match between the measured (symbols) and calculated (lines) values is established for the various angle ellipsometric spectra of S1 and S2 in the transparent region 400-1700 nm.The values of the fitting parameters are summarized in Table 1.

Table 1. Outputs ellipsometry simulation parameters (thickness, surface roughness, and Cauchy dispersion parameters A, B, C) related to samples S1 and S2. The values of each parameter are given with the same number of significant digits

Fitting parameters	Sample S1	Sample S2
MSE	4.895	7.062
Roughness (nm)	2.023	6.834
Thickness (μm)	1.4642±0.00242	1.6355± 0.00240
A	2.254±0.0022	2.274±0.0023
B	0.02624±0.001331	0.03587 ± 0.001772
C	0.00281±0.00018084	0.00213± 0.00025153

The SE-determined film thicknesses for S1 and S2 are within the accuracy of the average thickness obtained by UV-VIS measurements. A potential discrepancy in the dispersion of the ordinary and extraordinary refractive indices in the wavelength range under investigation could account for the tiny discrepancy between the experimental data and the model. Figure 6 compares the obtained refractive indices with those previously reported (Kawashima, 1997; Lian, 2003 and Kim, 2008).

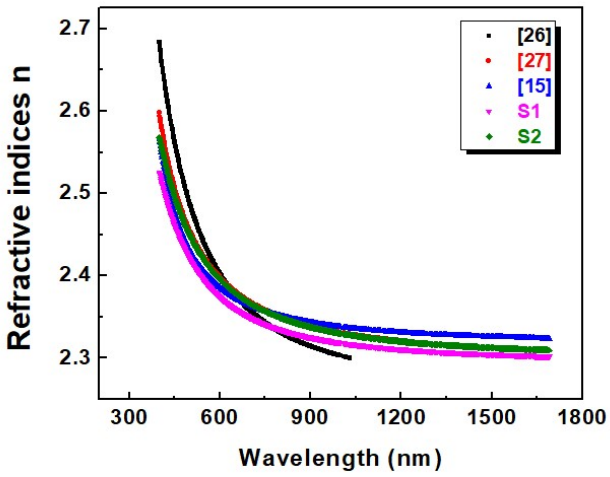

Figure 6. Extracted refractive indices as a function of λ for the samples with (S1) and without (S2) SiN treatment. (black diamond—[15], black square—[26], black circle—[27])

First, upon SiN treatment, the GaN refractive index blueshifts. This is well correlated with the energy gap blueshift observed in sample S1. Furthermore, upon SiN treatment, the GaN refractive index decreases. This behavior is explained by the improved crystal quality upon SiN treatment observed in the HRXRD results in the previous section. S1 and S2 have almost the same thickness and surface roughness.Thus, the variation in refractive indices is mainly due to the difference in dislocation density (Natali, 2003) suggested that the discrepancies in the different reported studies on the AlN refractive index are significantly affected by the strain level and dislocation density. This was experimentally proven by changing the growth conditions of AlN in reference (Joo, 2000). On the other hand, Ben *et al*. (2019), theoretically associated the change in the refractive index of AlN with the presence of a nanoscale strain field around dislocations. The decrease in the GaN refractive index upon SiN treatment is suggested to be related to the change in the local atomic environment due to the presence of dislocations. Furthermore, the common effects of SiN treatment on dislocations, point defects, and surface morphology cause difficulties in separating their coupled effects on refractive index variation.

Due to the SiN-specific effect on threading edge dislocation reduction, additional detailed further experimental and/or theoretical studies are needed to determine the effect ofSiN treatment on the GaN refractive index. In Figure 6, Lian et al. (2003) superimposed the GaN refractive index dispersion spectrum on sample S2's refractive index over a wide wavelength range (400-1200 nm). In the wavelength range from 400 nm to 650 nm, we found that the refractive index reported in reference (Kawashima, 1997) lies between the S1 and S2 spectra from our work. In Figure 6, we also plot the refractive index dispersion function reported by Tae et al. (Kim, 2008). We noted that their results lay between those of the S1 and S2 spectra in the short wavelength range. We speculate that Tae et al.'s (Kim, 2008) GaN samples were fabricated using a different growth method, molecular beam epitaxy, which may be the cause of this discrepancy.Surface parameters such as oxide overlayers, physisorbed pollution, and surface roughness all have a significant impact on SE readings. If the surface roughness is overlooked in the analysis of the SE spectra, significant mistakes in refractive index determination can occur even for roughness values as small as 5 nm. Most of the reported results on GaN refractive index dispersion did not provide information about the structural properties of the studied samples. Surface roughness, substrate back surface reflection, anisotropy, and crystal quality variations may be the causes of the discrepancies in the reported refractive index dispersion plots in Figure 6.

For greater accuracy, the SE findings were supported by the ex-situ normal incidence spectroscopy (SR) reflectivity in the wavelength range from 400 nm to 1000 nm. Figure 7 shows the reflection spectra of samples S1 and S2.

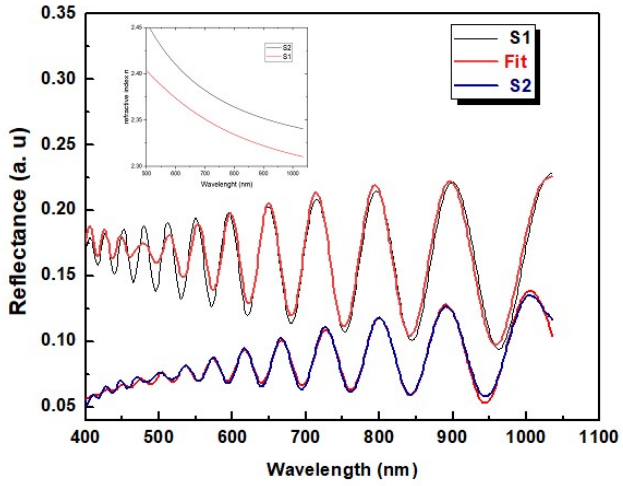

Figure 7. Reflectance spectra of samples S1 and S2. The red solid lines represen
the Cauchy-ty
nm for the two samples

****

The oscillation comes from the multireflected light interference from the air/GaN and GaN/sapphire interfaces. Based on interference theory and by using the thin filmetric F20 software provided within the experiment, the extracted film thicknesses are 1.448 μm and 1.634 μm for S1 and S2, respectively. Again, these findings are in good agreement with the above previous findings in the present work. A four-multilayer structure (air/roughness/GaN/sapphire) was used to fit the SR data. The best fit is shown in Figure 6. A more accurate fitting is performed for a wavelength greater than 500 nm. The Cauchy-type refractive indices determined in the range of 500 nm to 1000 nmare shown in the inset of Figure 6. We again noted a reduction in the refractive index of GaN upon SiN treatment. The refractive indices of the SE and SR measurements were comparable. Based on the discussion above, we think that one important aspect for determining the refractive index is the GaNgrowth conditions. Any design and study of GaN-based optoelectronic devices in the region near or close to the fundamental absorption edge of GaN must consider the refractive-index (n) dispersion.

CONCLUSION

The influence of sapphire SiN treatment on the optical and structural properties of GaNwas investigated by high-resolution X-ray diffraction, UV–vis spectroscopy, spectroscopy ellipsometry, and spectroscopy reflectivity. SiN treatment improved the crystal quality, as shown by the decrease in the symmetric and asymmetric rocking curve FWHM. Furthermore, the optical properties are enhanced, and the energy band gap shows a blueshift of approximately 10 meV.Excellent fitting of the SE measurements at three angles 55°, 60°, and 65°, wasaccomplished using the Cauchy dispersion equation,whichled to the determination of the GaN refractive index dispersion. In the wavelength range (400-1700 nm), SE measurements of the refractive index exhibited a blueshift and a decrease upon SiN treatment. This same tendency was proven by the SR in the wavelength range (500-1000 nm), confirming the SE results.

Author contributions

The authors confirm the contributions of the paper to the field as follows: Study conception and design: A. Bchetnia, J. Laifi; Epitaxial growth: A. Bchetnia; Characterization of samples: A. Bchetnia, Wateen Chalabi, T. Lafford; Analysis and interpretation of results: A. Bchetnia, J. Laifi, Wateen Chalabi. All the authors reviewed the results and approved the final version of the manuscript.

Data availability: The authors declare that the data supporting the findings of this study are available within the paper.

Competing interests: We have no competing interests to declare.

REFERENCES

Amano. H, Akasaki. I, Hiramatsu. K, Koide. N, & Sawaki. N. Thin Solid Films 163, 1988 415-420.

Amano. H, Sawaki. N, Akasaki. I, & Toyoda. Y. Applied Physics Letters, 48(5) 1986 353-355.

Bchetnia. A, Touré. A, Lafford. T.A, Benzarti. Z, Halidou. I, Habchi. M.M, El Jani. B. *Journal of Crystal Growth*, 308 (2), (2007) pp. 283-289.

Ben. J, Sun. X, Jia. Y, Jiang. K, Shi. Z, Wu. Y, Li. D. Nanoscale Research Letters, 14 (2019) 1-7.

Benzarti. Z, Halidou. I, Boufaden. T, El Jani. B, Juillaguet. S, & Ramonda. M physica status solidi (a), 201(3) (2004) 502-508.

Benzarti. Z, Sekrafi. T, Bougrioua. Z, Khalfallah. A, & El Jani. B. *Journal of Electronic Materials,* 46 (2017) 4312-4320.

Böttcher. T, Einfeldt. S, Figge. S, Chierchia. R, Heinke. H, Hommel. D & Speck. J. S. Applied Physics Letters, 78(14) 2001 1976-1978.

Edwards. A. P, Mittereder. J. A, Binari. S. C, Katzer. D. S, Storm. D. F & Roussos. *J. IEEE electron device letters,* 26(4) 2005 225-227.

Fitouri. H, Benzarti. Z, Haidou. I, Boufaden. T & El Jani. B. Phys. Stat. Sol. (a) 202 (13) (2005), 2467–2473.

Haffouz. S, Kirilyuk. V, Hageman. P. R, Macht. L, Weyher. J. L, & Larsen. P. K. Applied Physics Letters, 79(15) (2001) 2390-2392.

Joo. H. Y, Kim. H. J, Kim. S. J & Kim. S. Y. Thin solid films, 368(1) (2000) 67-73.

Jubu. P. R, Yam. F. K, Igba. V. M & Beh. K. P. Journal of Solid State Chemistry, 290 (2020) 121576.

Kawashima. T, Yoshikawa. H, Adachi. S, Fuke. S & Ohtsuka. K *Journal of applied physics,* 82(7) (1997) 3528-3535.

Kim. T. J, Byun. J. S, Kim. Y. D, Chang. Y. C & Kim. H. J. Journal of the Korean Physical Society, 53(3) (2008) 1575-1579.

Kyle, E.C, Kaun. S. W, Burke. P. G, Wu. F, Wu. Y. R, & Speck. J. S. *Journal of applied physics*, 115 (2014) 19.

Li. L, Yang. Y, Chen. G, Wang. W, Jiang. H, Wang. H & Li. G. Vacuum 197 (2022) 110800.

Lian. C. X, Li. X. Y & Liu. J. Semiconductor science and technology, 19 (3) (2003) 417.

Miyoshi, T., Masui, S., Okada, T., Yanamoto., T., Kozaki., T, Nagahama, S.I, & Mukai, T. *Applied Physics Express,* 2(6) (2009) 062201.

Nakamura. S. N. S. Japanese Journal of Applied Physics, 30(10A) (1991) L1705.

Natali. F, Semond. F, Massies. J, Byrne. D, Laügt. S, Tottereau. O& Dumont. E. Applied physics letters, 82(9) (2003) 1386-1388.

Panda. P, Ramaseshan. R & Sundari. S. T. Optical Materials, 118 (2021) 111245.

Siozade. L, Colard. S, Mihailovic. M, Leymarie. J, Vasson. A, Grandjean. N & Massies. J. Japanese Journal of Applied Physics, 39(1R) (2000) 20.

Sullivan. B. T, Parsons. R. R, Westra. K. L, & Brett. M. J. *Journal of applied physics,* 64(8) (1988) 4144-4149.

Vickers. M. E, Kappers. M. J, Datta. R, McAleese. C, Smeeton. T. M, Rayment. F. D. G & Humphreys. C. J. Journal of Physics D: Applied Physics, 38(10A) (2005) A99.

Vidal. M. A, Ramírez-Flores. G, Navarro-Contreras. H, Lastras-Martínez. A, Powell. R. C & Greene. J. E. Applied physics letters, 68(4) (1996) 441-443.

Yang. T, Goto. S, Kawata. M, Uchida. K, Niwa. A & Gotoh. J. Japanese journal of Applied Physics, 37(10A) (1998) L1105.

Yu. G, Wang. G, Ishikawa. H, Umeno. M, Soga. T, Egawa. T &Jimbo. T Applied Physics Letters, 70(24) (1997) 3209-3211.

Yu. G. Y. G, Ishikawa. H. I. H, Egawa. T. E. T, Soga. T. S. T, Watanabe. J. W. J, Jimbo. T. J. T & Umeno. M. U. M, Japanese *Journal of Applied Physics*, 36(8A) (1997) L1029.

Zauner. A. R. A, Devillers. M. A. C, Hageman. P. R, Larsen. P. K & Porowski. S. Materials Research Society, Internet Journal of Nitride Semiconductor Research, 3 (1998) e17.

Zhu. Q, Botchkarev. A, Kim. W, Aktas. Ö, Salvador. A, Sverdlov. B & Smith. D. J, Applied physics letters, 68(8) (1996)1141-1143.

****